



# Preferential Infiltration of Unique V $\gamma$ 9J $\gamma$ 2-V $\delta$ 2 T Cells Into Glioblastoma Multiforme

Mijeong Lee<sup>1,2†</sup>, Chanh Park<sup>3†</sup>, Jeongmin Woo<sup>4†</sup>, Jinho Kim<sup>4</sup>, Inseong Kho<sup>3</sup>, Do-Hyun Nam<sup>1,2,5</sup>, Woong-Yang Park<sup>1,4</sup>, Yeon-Soo Kim<sup>6</sup>, Doo-Sik Kong<sup>2,5\*</sup>, Hye Won Lee<sup>1,7,8\*</sup> and Tae Jin Kim<sup>1,3\*</sup>

<sup>1</sup> Department of Health Science and Technology, Samsung Advanced Institute for Health Science and Technology, Sungkyunkwan University, Seoul, South Korea, <sup>2</sup> Institute for Refractory Cancer Research, Samsung Medical Center, Seoul, South Korea, <sup>3</sup> Division of Immunobiology, Department of Molecular Cell Biology, Sungkyunkwan University School of Medicine, Suwon, South Korea, <sup>4</sup> Samsung Genome Institute, Samsung Medical Center, Seoul, South Korea, <sup>5</sup> Department of Neurosurgery, Samsung Medical Center, Sungkyunkwan University School of Medicine, Seoul, South Korea, <sup>6</sup> Department of New Drug Discovery and Development, Chungnam National University, Daejeon, South Korea, <sup>7</sup> Department of Anatomy and Cell Biology, Sungkyunkwan University School of Medicine, Suwon, South Korea, <sup>8</sup> Single Cell Network Research Center, Sungkyunkwan University, Seoul, South Korea

## OPEN ACCESS

### Edited by:

Carlos Barcia,  
Autonomous University of Barcelona,  
Spain

### Reviewed by:

Zsolt Sebestyen,  
University Medical Center Utrecht,  
Netherlands  
Levi Watkin,  
Baylor College of Medicine,  
United States

### \*Correspondence:

Doo-Sik Kong  
neurokong@gmail.com  
Hye Won Lee  
nsproper@naver.com  
Tae Jin Kim  
tjkim@skku.edu

<sup>†</sup>These authors have contributed  
equally to this work

### Specialty section:

This article was submitted to  
Cancer Immunity and Immunotherapy,  
a section of the journal  
Frontiers in Immunology

**Received:** 16 September 2018

**Accepted:** 01 March 2019

**Published:** 22 March 2019

### Citation:

Lee M, Park C, Woo J, Kim J, Kho I,  
Nam D-H, Park W-Y, Kim Y-S,  
Kong D-S, Lee HW and Kim TJ (2019)  
Preferential Infiltration of Unique  
V $\gamma$ 9J $\gamma$ 2-V $\delta$ 2 T Cells Into Glioblastoma  
Multiforme. *Front. Immunol.* 10:555.  
doi: 10.3389/fimmu.2019.00555

Glioblastoma multiforme (GBM) is clinically highly aggressive as a result of evolutionary dynamics induced by cross-talk between cancer cells and a heterogeneous group of immune cells in tumor microenvironment. The brain harbors limited numbers of immune cells with few lymphocytes and macrophages; thus, innate-like lymphocytes, such as  $\gamma\delta$  T cells, have important roles in antitumor immunity. Here, we characterized GBM-infiltrating  $\gamma\delta$  T cells, which may have roles in regulating the GBM tumor microenvironment and cancer cell gene expression. V(D)J repertoires of tumor-infiltrating and blood-circulating  $\gamma\delta$  T cells from four patients were analyzed by next-generation sequencing-based T-cell receptor (TCR) sequencing in addition to mutation and immune profiles in four GBM cases. In all tumor tissues, abundant innate and effector/memory lymphocytes were detected, accompanied by large numbers of tumor-associated macrophages and closely located tumor-infiltrating  $\gamma\delta$  T cells, which appear to have anti-tumor activity. The immune-related gene expression analysis using the TCGA database showed that the signature gene expression extent of  $\gamma\delta$  T cells were more associated with those of cytotoxic T and Th1 cells and M1 macrophages than those of Th2 cells and M2 macrophages. Although the most abundant  $\gamma\delta$  T cells were V $\gamma$ 9V $\delta$ 2 T cells in both tumor tissues and blood, the repertoire of intratumoral V $\gamma$ 9V $\delta$ 2 T cells was distinct from that of peripheral blood V $\gamma$ 9V $\delta$ 2 T cells and was dominated by V $\gamma$ 9J $\gamma$ 2 sequences, not by canonical V $\gamma$ 9J $\gamma$ P sequences that are mostly commonly found in blood  $\gamma\delta$  T cells. Collectively, unique GBM-specific TCR clonotypes were identified by comparing TCR repertoires of peripheral blood and intra-tumoral  $\gamma\delta$  T cells. These findings will be helpful for the elucidation of tumor-specific antigens and development of anticancer immunotherapies using tumor-infiltrating  $\gamma\delta$  T cells.

**Keywords:** glioblastoma multiforme, tumor immune microenvironment, gamma-delta T cells, gamma-delta T-cell receptor repertoire, immune repertoire sequencing

## INTRODUCTION

Glioblastoma multiforme (GBM) progresses by co-opting stromal cells that reside in or are recruited to the tumor microenvironment (TME), which is a complex ecosystem composed of heterogeneous tumor cells associated with extensive hypoxic zones, reactive astrocytes, and infiltrating distinct immune components, including microglia, tumor-associated macrophages (TAMs) derived from peripheral blood monocytes, granulocytes, myeloid-derived suppressor cells (MDSCs), and T cells (1–5). In particular, GBM tumor cells along with immune factors create a complex milieu, which ultimately leads to alteration of the tumor cell transcriptome and tumor evolution (6, 7). TAMs, the predominant immune population infiltrating GBMs (1, 8), orchestrates GBM evolution by facilitating the mesenchymal transition, neoangiogenesis, extra-cellular matrix remodeling, and immune modulation (6, 9–11). Furthermore, accumulation of CD4<sup>+</sup> T helper (Th) cells and CD4<sup>+</sup>CD25<sup>+</sup> transcription factor forkhead box P3 (FoxP3)<sup>+</sup> regulatory T cells (Tregs) combined with the reduced presence of CD8<sup>+</sup> cytotoxic T cells results in curtailment of immunotherapeutic efficacy (9, 12).

However, the nature of GBM-infiltrating  $\gamma\delta$  T cells has not been extensively investigated, although  $\gamma\delta$  T cells have the potential to kill cancer cells and to change the pro-tumoral TME to one favoring acute responses and potent anti-tumoral activity. (13–19). The human TCR variable (V) regions of TCR  $\gamma$  and  $\delta$  genes contains 14 unique V $\gamma$  segments (TRGV), three unique V $\delta$  segments (TRDV1, TRDV2, and TRDV3), and five V $\delta$  segments that share a common nomenclature with V $\alpha$  segments (TRDV4/TRAV14, TRDV5/TRAV29, TRDV6/TRAV23, TRDV7/TRAV36, and TRDV8/TRAV38–2) (20). In healthy human adults, circulating T lymphocytes include 1–3%  $\gamma\delta$  T cells, most of which are V $\gamma$ 9V $\delta$ 2 T cells (16). V $\gamma$ 9V $\delta$ 2 T cells are activated by pyrophosphate-containing metabolites, generically known as phosphoantigens (pAgs), which are derived from microbes or metabolically active tumor cells and bind to the intracellular domain of the butyrophilin-related molecule BTN3A1 without major histocompatibility complex (MHC)- or CD1-dependent antigen presentations (18, 21). Especially, isopentenyl pyrophosphate (IPP) is a pAg generated from the mevalonate pathway in mammalian cells (22), and V $\gamma$ 9V $\delta$ 2 T cells have additional sensor for detecting cancer cells via recognition of IPP accumulated intracellularly during dysregulated metabolism in cancer cells (16–18, 23). GBM cancer cells also express several MHC-like stress-induced self-antigens (MIC-A/B), heat shock protein-60, U16-binding protein 4, human MutS homolog 2, and F1-ATP synthase, which are recognized by TCRs, Toll-like receptors, or natural killer (NK) receptors expressed on V $\gamma$ 9V $\delta$ 2 T cells, triggering cancer cell killing without any prior antigen exposure or priming (15, 24–26). Although the  $\gamma\delta$  T cell proliferative function is impaired in patients with GBM, *ex vivo*-expanded/activated  $\gamma\delta$  T cells from healthy donors are highly cytotoxic to GBM tumor cells (14), suggesting a therapeutic effects of the adoptive transfer of V $\gamma$ 9V $\delta$ 2 T-cells as an alternative immunotherapeutic strategy GBMs (13, 19). For example, temozolomide (TMZ)-induced

DNA damage upregulates NKG2D ligands on cancer cells that are vulnerable to V $\gamma$ 9V $\delta$ 2 T cell-mediated lysis in GBM (27).

Immune repertoire sequencing (IR-SEQ) can offer a comprehensive snapshot of the complexity and the diversity of the TCR repertoire (28, 29). There are many advantages of studying the TCR $\gamma\delta$  repertoire compared with repertoires of TCR $\alpha\beta$  and B-cell receptors because of relatively limited diversity of  $\gamma\delta$  T cells and their independence from different MHC haplotypes (30). In the blood, the repertoire of V $\gamma$ 9V $\delta$ 2 T cells is skewed toward cells expressing a biased V $\gamma$ 9 chain with V $\gamma$ 9-J $\gamma$ P-C1 rearrangement, which involves V $\gamma$ 9 gene segment, J $\gamma$ P (J $\gamma$ 1.2) joining segment, and C $\gamma$ 1 exon (31, 32). The V $\gamma$ 9-J $\gamma$ P-C1 chain is paired mainly with V $\delta$ 2 chains (31). Despite using common V-(D)-J rearrangements, circulating V $\gamma$ 9V $\delta$ 2 cells are still diverse due to the existence of D fragments, N-addition occurring during V-(D)-J recombination, and alternative rearrangement with the C $\gamma$ 2 segment (33, 34). In this study, we analyzed GBM-infiltrating  $\gamma\delta$  T cells with unique repertoire diversity although  $\gamma\delta$  T cells may be important innate lymphocytes modulating GBM TME. To evaluate the identity of central nervous system (CNS)-resident  $\gamma\delta$  T cells and determine whether blood  $\gamma\delta$  T cells were recruited to the tumor or whether local CNS-resident  $\gamma\delta$  T cells responded to the tumor, we performed  $\gamma\delta$  TCR repertoire analyses using tumor tissue and matched peripheral blood from four patients with GBM based on IR-SEQ technology.

## MATERIALS AND METHODS

### Sample Collection and Preparation for Repertoire Sequencing

We recruited four cohorts of patients diagnosed with GBM. All patients signed informed consent for the use of patients' samples for research purposes under protocols approved by the Samsung Medical Center Institutional Review Board (IRB no. 2016-11-073). Tumor tissues were stored in liquid nitrogen, and peripheral blood mononuclear cells (PBMCs) were isolated from whole blood with a Ficoll Histopaque gradient. PBMCs were labeled with fluorescein isothiocyanate-conjugated anti-CD45 antibodies (347463; BD Biosciences, San Jose, CA, USA), and CD45<sup>+</sup> cells were acquired using a BD FACS AriaIII flow cytometer with FACSDiva software (BD Biosciences).

### Panel Sequencing Data Analysis

Samples were profiled using GliomaSCAN, a sequencing platform designed to target 312 genes specific for GBM, at the Samsung Medical Center. These target genes were chosen by literature mining or requested by the researchers and clinicians. The paired-end reads were aligned to the human reference genome (hg19) using Burrows-Wheeler Alignment tool (version 0.7.5). We converted sequence alignment and mapping (SAM) files into binary alignment and mapping (BAM) files using SAMtools (version 0.1.19) followed by reads sorting. Duplicated reads were removed from BAM files with Picard (version 1.128; <http://broadinstitute.github.io/picard>). Local realignment of reads around potential small indels and base quality score recalibration was performed with the Genome Analysis Toolkit

(GATK, version 3.5.0) using dbSNP (build ID 137). Single nucleotide variants and indels were called using muTect2 (GATK version 3.8.0) and Strelka2 (version 2.8.2) with default parameter settings. The union of the variants identified by the two callers was used as the candidate variants. Variants were annotated using ANNOVAR. Variants located in exonic regions with a variant allele frequency of  $\geq 0.1$  were chosen for further investigation.

## Whole-Transcriptome Sequencing (WTS) and Enumeration of Immune Cell Subsets From WTS

Total RNA from human tissue was isolated with an RNeasy mini kit (#74106; Qiagen, Hilden, Germany). The biospecimens used for this study were provided by Samsung Medical Center BioBank (IRB no. 2016-11-073). For all samples, RNA-Seq libraries were prepared from 500 ng total RNA using an Illumina TruSeq RNA Sample Prep kit. All libraries were sequenced to a read depth of more than 75 million reads using an Illumina HiSeq2000 instrument to generate paired reads ends with a total read length of 100 bp. After trimming poor-quality reads and adapter sequences from the FASTQ files for each sample, we aligned the reads to the human reference genome (hg19) using STAR (version 2.5.0i) with two pass default mapping mode (35). With the same reference genome used for mapping, gene annotation data obtained from Ensemble (v 74) were used to quantify aligned reads. Transcripts per million normalized values for each gene were calculated based on total gene read counts and the lengths of merged exons using RSEM (version 1.2.17) (36). *In silico* deconvolution analysis was performed with transcriptomic data using the CIBERSORT algorithm under the default mode (37). The proportions of 22 immune cell types, including seven T-cell types, naïve and memory B cells, plasma cells, NK cells, and myeloid subsets were estimated using LM 22 datasets, which included the public gene signature matrix of 547 genes to distinguish 22 leukocyte subsets.

## Immune Cell Signature Analysis

Using curated immune gene expression signature (as shown in **Supplementary Table 1**) (38–41), gene set variation analysis (GSVA) was implemented to calculate sample wise enrichment scores for each immune related gene set using the Bioconductor package ‘GSVA’ (42) based on the TMM normalized WTS data from four GBM samples used in this study and TCGA-GBM dataset. GSVA scores were scaled and plotted using heatmap.2 function from *ggplot2* (43). RPKM normalized RNA-seq datasets for 170 samples from TCGA were used for GSVA analysis. Interrelations of all possible pairs of GSVA scores of Immune signature and gene expression values of  $\gamma\delta$  T cell related genes were estimated from Pearson’s correlation coefficient ( $r$ ). To infer significance of each correlation,  $P$ -values were calculated based on asymptotic  $t$  approximation. Hierarchical clustering of immune signature gene sets (column) and  $\gamma\delta$  T cell related gene expressions (row) was performed via Pearson’s correlation to measure distance with complete linkage algorithm for clustering distances.

## Library Preparation and Sequencing

The human TCR $\gamma$  and TCR $\delta$  CDR3 regions were amplified using the commercially available iRepertoire platform (iRepertoire Inc., Huntsville, AL, USA) in LAS Inc. (Kimpo, Gyeonggi-do, Korea). Briefly, total RNA samples were subjected to reverse transcription polymerase chain reaction (PCR) using iR-PCR1 Rxn Mix (iRepertoire Inc.) and PCR1 Rxn Mix (iRepertoire Inc.). The PCR product was purified using PCR1 Rescue Mix (iRepertoire Inc.). A second PCR was then carried out using PCR2 Mix again and the product was purified using PCR2 Clean-up Mix (iRepertoire Inc.). Finally, quality and band size of libraries were assessed using an Agilent 2100 bioanalyzer (Agilent, Santa Clara, CA, USA). Libraries were quantified by quantitative PCR using CFX96 Real Time System (Bio-Rad, Hercules, CA, USA). After normalization, sequencing of the prepared library was conducted on the Miseq system (Illumina, San Diego, CA, USA) with 250-bp paired-end reads.

## Analysis of the TCR Repertoire With High-Throughput Sequencing

Using an Illumina MiSeq system, we obtained 250-bp paired-end reads files, and the raw paired-end fastq files were analyzed using the Immune Repertoire High-throughput Sequence Analysis (IRSA) workflow at the iRepertoire website (<https://irweb.i repertoire.com/nir/>). The IRSA workflow included storing and managing sequencing data, removing sequencing artifacts, mapping reference sequences using the Smith-Waterman algorithm, identifying CDR3 junctions, and generating various distribution plots, such as domain usage, nucleotide nibbling, addition at the junction sites, and CDR3 length. Contigs of TCR constant genes were screened within quality control-filtered RNA-Seq data using the K-mer search algorithm of BBDuk program from the BMAP 35.74 suite (<http://sourceforge.net/projects/bbmap/>) with the parameter “ $k = 25$  edist = 2”. Constant genes for  $\alpha$ -,  $\beta$ -,  $\gamma$ -, and  $\delta$ -type TCRs used for the query were obtained from IMGT/LIGM-DB version 1.2.4 (44). Accession code X02883 was used to retrieve the *TRAC* gene of TCR $\alpha$ ; M12887 and L36092 for exons 1 and 2 of *TRBC1*; M12888 and L36092 for two exons of the *TRBC2* gene of TCR $\beta$ ; M14996, M14997, and M14998 for three exons of *TRGC1*; M14002 for *TRGC2* of TCR $\gamma$ ; and M22149, M22150, and M22151 for three exons of *TRDC1* of TCR $\delta$ . Additionally, TCR Repertoire Utilities for Solid Tissue (45) was used to detect TCR sequences from RNA-Seq data for individual samples.

## Immunohistochemistry (IHC)

IHC staining was performed using Opal<sup>TM</sup> 7-color manual kit (NEL81100KT, PerkinElmer, MA, USA) according to the manufacturer’s protocol (2014;70:46–58). Briefly, the slides were deparaffinized in xylene and rehydrated in ethanol. Antigen retrieval was performed in tris-buffered saline buffer (pH 9.0) using microwave treatment (MWT). Using two antibodies are listed as follow: TCR gamma/delta antibody (2  $\mu$ g/mL, mouse monoclonal, (5A6.E9), TCR1061, ThermoFisher, MA, USA) and CD204 (1  $\mu$ g/mL, rabbit polyclonal, ab64693, abcam, Cambridge, UK). These two antibodies were incubated 30 min in a humidified chamber at room temperature, followed by detection using

the mouse/rabbit SuperPicture Polymer Detection HRP kit. Visualization of the primary antibody was accomplished using each Opal Fluorophore Working Solution (TSA, 1:100), after which the slide was placed in tris-buffered saline buffer (pH 9.0) and repeated using MWT. TCR gamma/delta and CD204 were visualized with opal 690 and 520, respectively. Nuclei were subsequently visualized with DAPI and the slide was coverslipped using the antifade mounting solution (ADI-950-260-0025, Enzo, NY, USA). The slides were examined with Vectra Polaris Automated Quantitative Pathology Imaging System (PerkinElmer). InForm image analysis software (PerkinElmer) was used to analyze the spectra for all fluorophores included from 420 to 720 nm.

## Availability of Data and Material

Newly generated GliomaSCAN, WTS, and  $\gamma\delta$  TCR repertoire-Seq data from this study can be accessed at the European Genome-phenome Archive with accession number EGAS00001002790.

## RESULTS

### Clinical Presentation of Four Patients With Isocitrate Dehydrogenase (IDH) 1 Wild-Type GBM

The patients' clinical course and therapeutic protocols are summarized in **Supplementary Figure 1** and **Table 1**. Confirmation of IDH1 wild-type, O<sup>6</sup>-methylguanine-DNA-methyltransferase (MGMT) promoter-unmethylated GBM was made using R132 sequencing and methylation-specific PCR according to the 2016 World Health Organization criteria (46) after gross total resection (GTR). Four cases of GBM showed different genetic mutations with no mutation in the *IDH1* gene (**Figure 1A**). The first patient (case 1) was a 52-year-old woman with a large abnormal enhanced mass on the right temporal lobe on brain magnetic resonance imaging (MRI). She received concurrent chemoradiotherapy with TMZ followed by adjuvant TMZ (localized brain radiotherapy, total 60 Gy in 2 Gy per daily fraction with daily 75 mg/m<sup>2</sup> TMZ over 6 weeks followed by adjuvant cycles of TMZ 150 mg/m<sup>2</sup>/day for 5 days during each 28-day cycle) (47), and brain MRI during four adjuvant TMZ courses revealed tumor recurrence around the resection site. For chemotherapy against recurrent GBM, she was treated with bevacizumab 10 mg/kg and irinotecan 125 mg/m<sup>2</sup>. The second patient (case 2) was a 70-year-old man suffering from left temporo-occipital GBM with MGMT promoter-unmethylation. The GTR of the primary tumor was confirmed on the post-operative follow-up brain MRI. After concurrent chemoradiation and two adjuvant TMZ courses, newly developed multifocal nodular enhancing lesions at the subependymal area of both lateral ventricles suggesting leptomeningeal seeding were found. Bevacizumab 10 mg/kg and irinotecan 125 mg/m<sup>2</sup> were administered. The third patient (case 3) was a 60-year-old woman with a right temporal GBM with MGMT promoter-methylation. After GTR of the primary tumor was performed, she was treated with concurrent

chemoradiotherapy with TMZ followed by adjuvant TMZ with no obvious disease relapse during the follow-up period of 10 months. Final fourth patient (case 4) had a left temporo-parietal GBM with MGMT promoter-methylation. She received standard concurrent chemoradiation plus adjuvant TMZ with no obvious disease relapse during the follow-up period of 14 months.

### Abundant Infiltration of Macrophages and Innate and Effector/Memory Lymphocytes in GBM Tumor Tissues

To estimate antitumor immunity in GBM pathogenesis, we obtained gene expression profiles of four GBM tissues and measured the relative proportions of various immune cells through *in silico* deconvolution analysis (CIBERSORT; see **Supplementary Figure 2**). In all four cases, heavy infiltration of macrophages (32.0–80.3% of all immune cells), particularly M2 macrophages, and mast cells (6.7–34.6% of all immune cells) was noted. T and NK cells constituted about 5.6–31.0% of all immune cells, and most tumor-infiltrating lymphocytes (TILs) were innate and effector/memory cells, whereas naïve T cells were scarce. However, the enumeration of tumor-infiltrating  $\gamma\delta$  T cells via the CIBERSORT algorithm was difficult since  $\gamma\delta$  T cells also express most genes expressed in  $\alpha\beta$  T cells and NK cells (37, 48). Alternatively, the ratios of  $\gamma\delta$  T to  $\alpha\beta$  T cells were calculated to be around 0.8–1.1 by measuring the reads per kilobase of transcript per million mapped reads (RPKM) values of the *Tcrd* and *Tcrb* constant regions, suggesting that the ratios of  $\gamma\delta$  T cells were equal to or even higher than those of  $\alpha\beta$  T cells in the tumor tissues (**Figure 1B**). The case 3 showed the highest ratio of  $\gamma\delta$  T cells than the other cases, whereas the case 4 showed a lower ratio of  $\gamma\delta$  T cells than other cases.

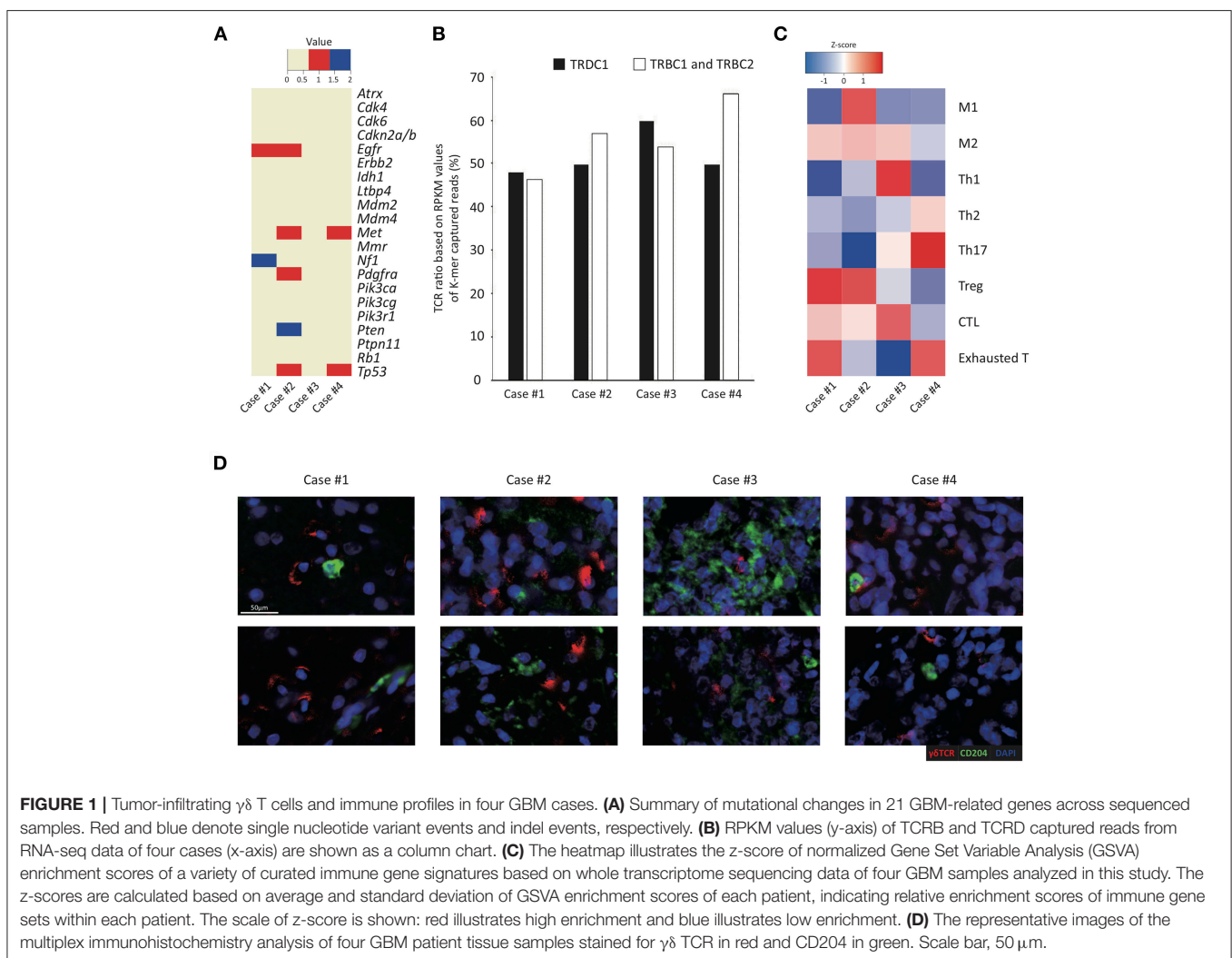
To explore the effects of  $\gamma\delta$  T cell infiltration, the phenotype of immune cells within the TME in four GBM samples was then analyzed based on multiple gene sets curated from various sources (summarized in **Supplementary Table 1**). In all four cases, heterogeneous and complex activation status of specific tumor-associated immune subsets modulating pro- or anti-tumor activity was demonstrated in each case. Notably, a relatively high abundance of cytotoxic T cell and Th1 genes was detected in case 3, which showed the highest ratio of  $\gamma\delta$  T cells over  $\alpha\beta$  T cells (**Figure 1C**). In contrast, case 4 tumor samples highly expressed Th17 and exhausted T cell genes compared to other samples. In case 1, genes related to M2 macrophage, Treg and exhausted T cells shaping immune-suppressive TME were relatively upregulated (**Figure 1C**). In further IHC study by using deparaffinized section slides,  $\gamma\delta$  T cells and TAMs were abundantly distributed throughout the tumor in all four cases and  $\gamma\delta$  T cells and macrophages were closely associated (**Figure 1D**).

We presumed that the abundance of  $\gamma\delta$  T cells may be correlated with TME, but we could not draw clear conclusion due to small sample sizes. To overcome this limitation, we further examined patient populations from the published dataset from TCGA RNA-seq ( $N = 170$ ) (**Figure 2**). Interestingly, the gene signature score of  $\gamma\delta$  T cells more positively correlated with those of M1 macrophages and Th1 cells than those of M2 macrophages

**TABLE 1** | Clinical characteristics of four glioblastoma patients.

Case	Age	Gender	Tumor location	MGMT promoter methylation status	Post-adjuvant treatment	PFS (Days)	OS (Days) (all censored)
#1	52	Female	Rt. T	Un-methylated	Radiotherapy plus concomitant and adjuvant temozolomide	207 (progression during F/U)	270
#2	70	Male	Lt. T-O	Un-methylated	Radiotherapy plus concomitant and adjuvant temozolomide (#2) + Bevacizumab plus irinotecan after disease recurrence	144 (progression during F/U)	173
#3	60	Female	Rt. T	Methylated	Radiotherapy plus concomitant and adjuvant temozolomide	198 (Censored, no progression during F/U)	198
#4	61	Female	Lt. T-P	Methylated	Radiotherapy plus concomitant and adjuvant temozolomide	249 (Censored, no progression during F/U)	249

Lt., left; Rt., right; T-P, temporo-parietal; T, temporal; T-O, temporo-occipital; GTR, gross total resection; IDH1, Isocitrate dehydrogenase 1; WT, wild type; MGMT, O6-methylguanine-DNA-methyltransferase; RT, radiotherapy; TMZ, temozolomide; PFS, progression-free survival; OS, overall survival; F/U, follow-up.



and Th2 cells, respectively. Notably, the  $\gamma\delta$  T cell activity was strongly associated with cytotoxic T cell activity, suggesting that GBM-infiltrating  $\gamma\delta$  T cells contribute to anti-tumoral immunity.

However, the  $\gamma\delta$  T cell activity was also associated with the activities of exhausted and regulatory T cells. These findings are consistent with previous findings demonstrating that  $\gamma\delta$  T cells

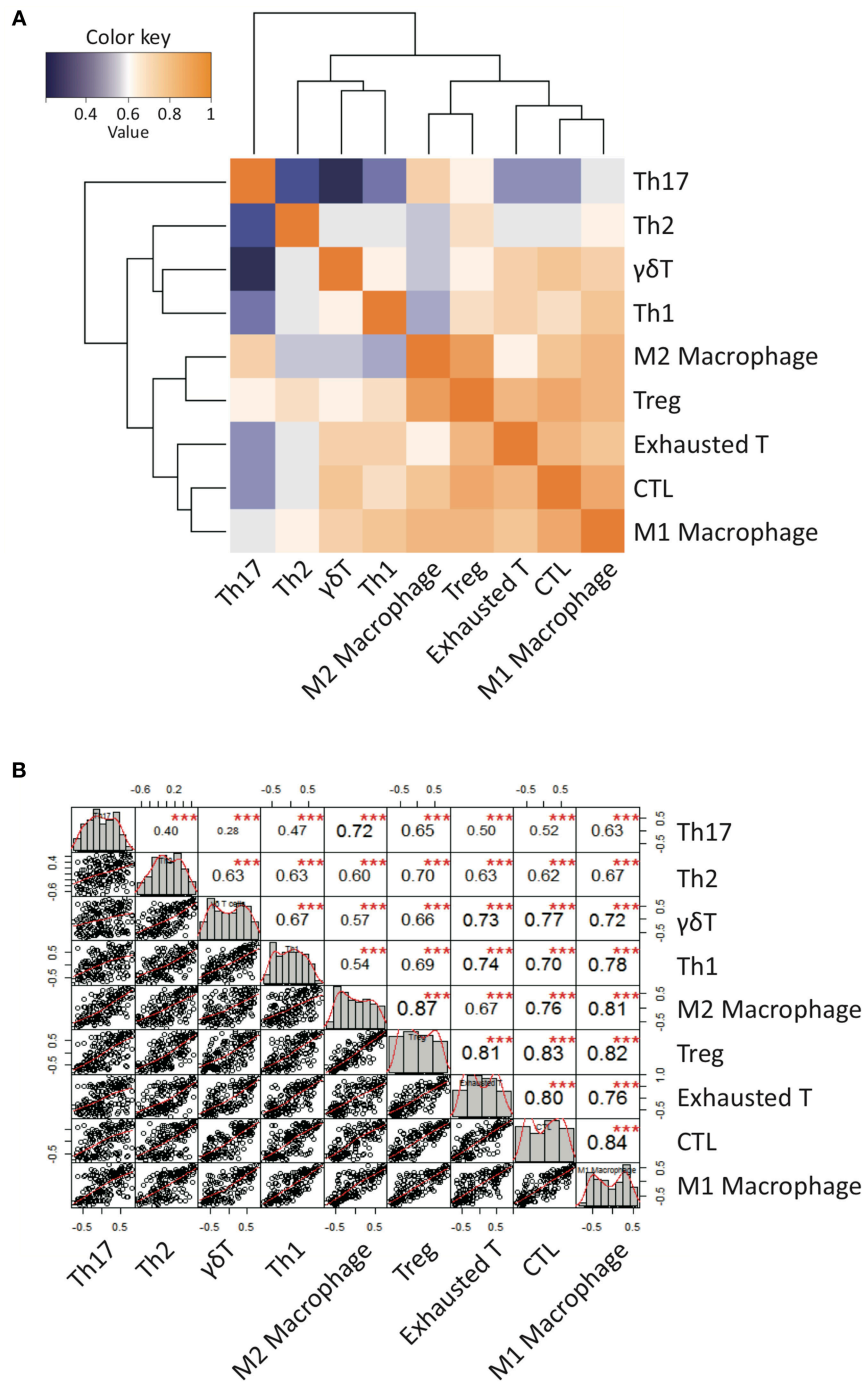


**FIGURE 2 |** Correlation patterns of Gene Set Variable Analysis (GSVA) enrichment scores of a variety of curated immune gene signatures for 170 GBM patients from TCGA database. **(A)** A clustered heatmap of Pearson's correlation coefficient of GSVA scores over all immune signature gene sets. Hierarchical clustering was performed based on Pearson's correlation distance with ward linkage method. Dark orange denotes high correlation ( $r = 1$ ) while dark blue denotes a lack of correlation ( $r > 0$ ). **(B)** The diagonal of the chart represent distribution of GSVA enrichment scores. The bivariate scatter plots of linear regression fits of each pairs with the fitted lines are shown on the bottom of the diagonal. Pearson's correlation coefficient values with the level of significance were shown on the top of the diagonal. \*\*\* $P < 0.001$ .

show a high degree of plasticity and are able to assume different phenotypes, including Th1-like, Th2-like, Th17-like, follicular Th-like, or Treg-like characteristics, depending on the cytokine

milieu in surrounding microenvironment (49–55). Based on the hypothesis that the  $\gamma\delta$  T cells could be responsible for the polarization of TAMs, we performed repertoire analyses of

$\gamma\delta$  T cells since individual subsets of  $\gamma\delta$  T cells with specific variable domains of  $\gamma$  or  $\delta$  chains have unique functions in local environments.

## Predominant Infiltration of $V\gamma9V\delta2$ T Cells in GBM Tumor Tissues

To compare  $\gamma\delta$  TCR repertoires between tumor-infiltrating and blood  $\gamma\delta$  T cells and among  $\gamma\delta$  T cells from four patients, we generated and amplified *Tcr $\gamma$*  and *Tcr $\delta$*  cDNA libraries from tumor tissues and sorted ( $2 \times 10^5$  to  $8 \times 10^6$ ) blood  $CD3^+$  cells from four patients. The libraries, which could be distinguished by barcodes, were then pooled and sequenced (Illumina MiSeq). In total, 159,138–2,483,772 total clean nucleotide sequences (CNTs) and about 141–1,157 unique clean nucleotide sequences (CNU) from the tumor samples and 402,922–2,145,312 CNTs and 93–2,709 unique CNU from the sorted blood  $CD3^+$  cells were analyzed in this study (Table 2). The *TCRG* and *TCRD* tree maps for each  $\gamma\delta$  T cell population showed that intratumoral  $\gamma\delta$  T cells expressed less diverse CDR3 nucleotide sequences for the *TCRG* and *TCRD* genes than blood  $\gamma\delta$  T cells, except in case 3 (Figures 3A,B). Case 3 showed oligoclonal  $\gamma\delta$  T cells in both blood and tumor tissue. The calculation of Shannon indices, which reflected both richness and evenness of the CDR3 clonotypes, showed that the repertoires of *TCRG* and *TCRD* CDR3 sequences were very restricted in case 3 and that the intratumoral  $\gamma\delta$  T cells were less diverse than blood  $\gamma\delta$  T cells (Table 2). In all cases, the most abundant  $\gamma\delta$  T cells were of  $V\gamma9$  and  $V\delta2$  cells.

## Unique $V\gamma9J\gamma2$ - $V\delta2$ T Cells Were Distinctively Found in GBM Tumor Tissues, but Not in Blood

$V\gamma9V\delta2$  T cells are known to be the most abundant type of adult blood  $\gamma\delta$  T cells (56). These cells undergo rapid expansion within the first year of life (57). Because  $V\gamma9V\delta2$  T cells are strongly

activated by bacteria-derived pAgs (18, 21), these cells appear to be expanded by commensal bacteria (18). A few previous TCR repertoire analyses have revealed the predominance of canonical  $V\gamma9J\gamma P$  sequences (58). Although intratumoral and blood  $V\gamma9V\delta2$  T cells were apparently similar, the Jensen-Shannon divergence (JSD) indices, a measure of repertoire comparison (59), showed remarkable distinctness of intratumoral  $\gamma\delta$  T cells from blood  $\gamma\delta$  T cells (Table 2). Notably, in case 3, intratumoral  $\gamma\delta$  T cells were completely distinct from blood  $\gamma\delta$  T cells (JSD = 1 indicates complete divergence of two repertoires). When we plotted the clonotypes based on  $V\gamma$  and  $J\gamma$  segments, the absolute or relative abundance of  $V\gamma9J\gamma2$  sequences was prominent in intratumoral  $\gamma\delta$  T cells, except in case 4 (Figure 4). The canonical  $V\gamma9J\gamma P$  sequences were the most abundant sequences in blood  $\gamma\delta$  T cells, except in case 4. Case 4 was unique in that many non-canonical  $V\gamma9J\gamma1$ ,  $V\gamma9J\gamma2$ ,  $V\gamma9J\gamma P1$ , and  $V\gamma9J\gamma P2$  sequences as well as the canonical  $V\gamma9J\gamma P$  sequences were found in blood  $\gamma\delta$  T cells, as was verified through repetitive sequencing analysis. Paradoxically, the canonical  $V\gamma9J\gamma P$  sequences were the most abundant in intratumoral  $\gamma\delta$  T cells from case 4. Collectively, the non-canonical  $V\gamma9J\gamma2$ - $V\delta2$  T cells were distinctively observed in intratumoral  $\gamma\delta$  T cells in three of four GBM cases.

## Unique CDR3 $V\gamma9J\gamma2$ and $V\gamma9J\gamma P$ Clonotypes From GBM Tumor Tissues and Blood

To date, it is unclear whether there were variations in TCR  $V\gamma9$   $\gamma$  chains related to antigenic specificity. In this study, we attempted to identify shared clonotypes that were found in different samples, although the antigenic specificity could not be deduced from the sequences. We reasoned that clonotypes of tumor phospho-antigen-specific  $V\gamma9V\delta2$  T cells may be different from blood bacterial phospho-antigen-specific  $V\gamma9V\delta2$  T cells. We listed the top 10 CDR3 clonotypes of canonical  $V\gamma9J\gamma P$  or non-canonical  $V\gamma9J\gamma2$  sequences from four blood and tumor samples (Table 3). We found that the  $V\gamma9J\gamma P$  CDR3 clonotype ALWEVQELGKKIKV was the most frequent clonotype in blood and tumor samples from three cases, suggesting that this was the most representative clonotype of canonical  $V\gamma9J\gamma P$   $\gamma$  chains. However, other frequent  $V\gamma9J\gamma P$   $\gamma$  chain CDR3 clonotypes were also found, such as ALWEPPQELGKKIKV, in both blood and tumor samples from only case 1, ALWEKQELGKKIKV in the blood sample from case 2, and ALWEALRLGKKIKV in blood and tumor samples from case 3. Notably, we found several frequent  $V\gamma9J\gamma2$   $\gamma$  chain CDR3 clonotypes that were unique to tumors and were not found in blood. The representative  $V\gamma9J\gamma2$   $\gamma$  chain clonotypes included ALWEGLKKL in case 1, ALWEVQYKKL in case 2, ASKKTKKL in case 3, and ALWEVRYYYKKL in case 4. In case 2, ALWESSNYKKL was a  $V\gamma9J\gamma2$   $\gamma$  chain clonotype found only in the blood. Collectively, we could discern unique blood- and tumor-specific  $V\gamma9$   $\gamma$  chain CDR3 clonotypes and found that many tumor-specific clonotypes were of  $V\gamma9J\gamma2$   $\gamma$  chains, and many blood-specific clonotypes were of  $V\gamma9J\gamma P$   $\gamma$  chains. In particular, the  $V\gamma9J\gamma P$  CDR3 clonotype ALWEVQELGKKIKV appeared to be the most representative  $V\gamma9J\gamma P$   $\gamma$  chains. The  $\gamma\delta$  T cells with

TABLE 2 |  $\gamma\delta$  T cell receptor repertoire diversity indices.

Case #	TCR chain	Cell origin	Shannon index	Janssen-Shannon divergence
#1	$\gamma$ chain	PBMCs	6.841	0.738
		Cancer tissue	6.087	
	$\delta$ chain	PBMCs	7.599	
		Cancer tissue	5.156	
#2	$\gamma$ chain	PBMCs	5.665	0.543
		Cancer tissue	4.736	
	$\delta$ chain	PBMCs	6.069	
		Cancer tissue	4.467	
#3	$\gamma$ chain	PBMCs	1.458	1
		Cancer tissue	3.270	
	$\delta$ chain	PBMCs	0.624	
		Cancer tissue	0.661	
#4	$\gamma$ chain	PBMCs	5.301	0.795
		Cancer tissue	4.609	
	$\delta$ chain	PBMCs	3.612	
		Cancer tissue	2.905	

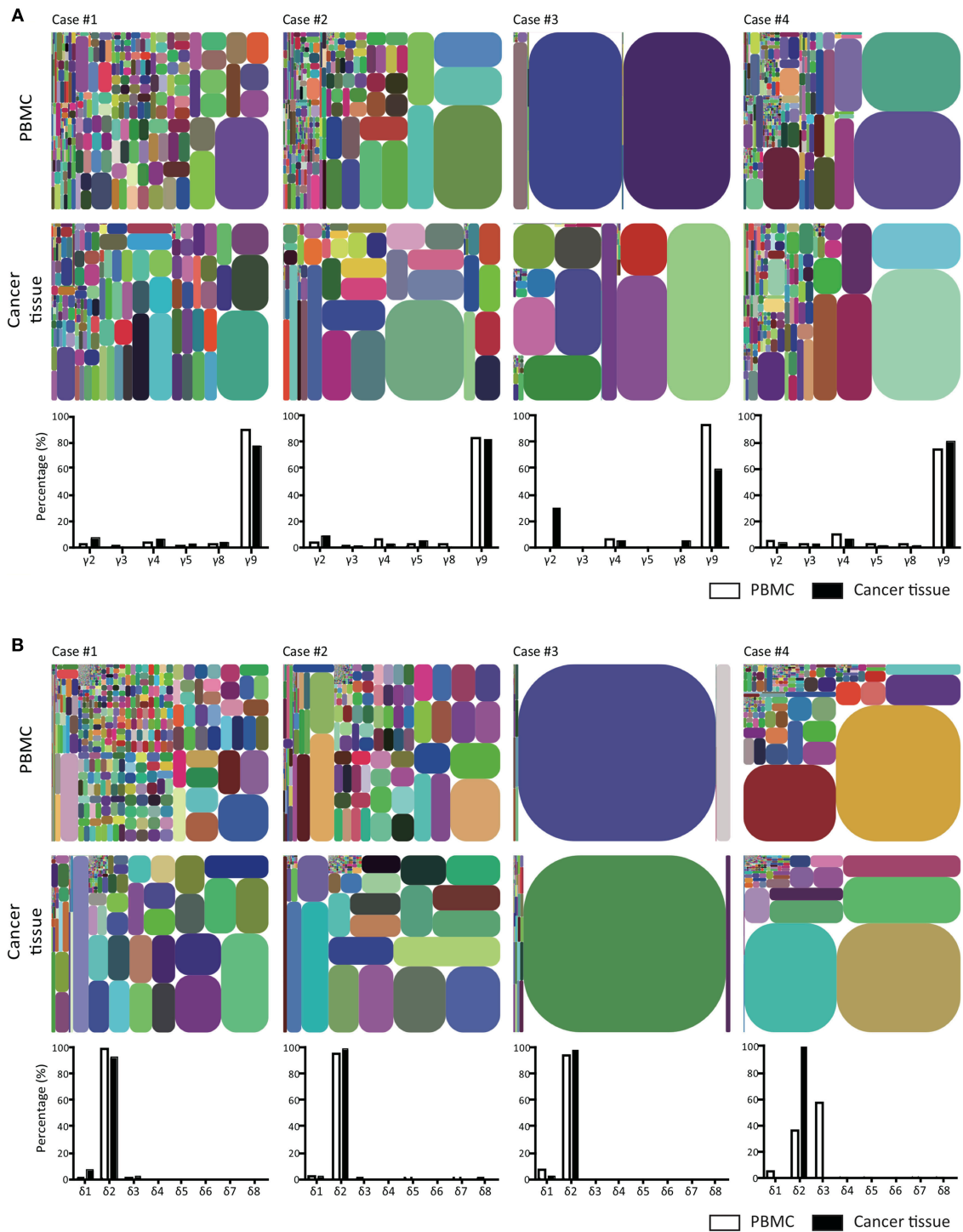


**FIGURE 3 |** T cell receptor  $\gamma$  and  $\delta$  chain CDR3 tree map plots for blood and GBM tumor tissue  $\gamma\delta$  T cells and the relative proportions of individual TCR  $\gamma$  or  $\delta$  gene segments. **(A)** for TCR $\gamma$  **(B)** for TCR $\delta$ . CDR3 tree-map plots illustrate the unique TCR $\gamma$  or TCR $\delta$  CDR3 nucleotide sequences obtained from given samples of four GBM patients. Each rectangle in a given tree-map represents a unique CDR3 sequence, and the size of each rectangle indicates the relative frequency of an individual sequence. The colors for the individual CDR3 sequences in each tree-map plot were chosen randomly. Bottom graphs in **(A,B)** show the percentages of use of each TCR  $V\gamma$  **(A)** or  $V\delta$  **(B)** domain in PBMCs (white) or cancer tissues (black) from each patient.



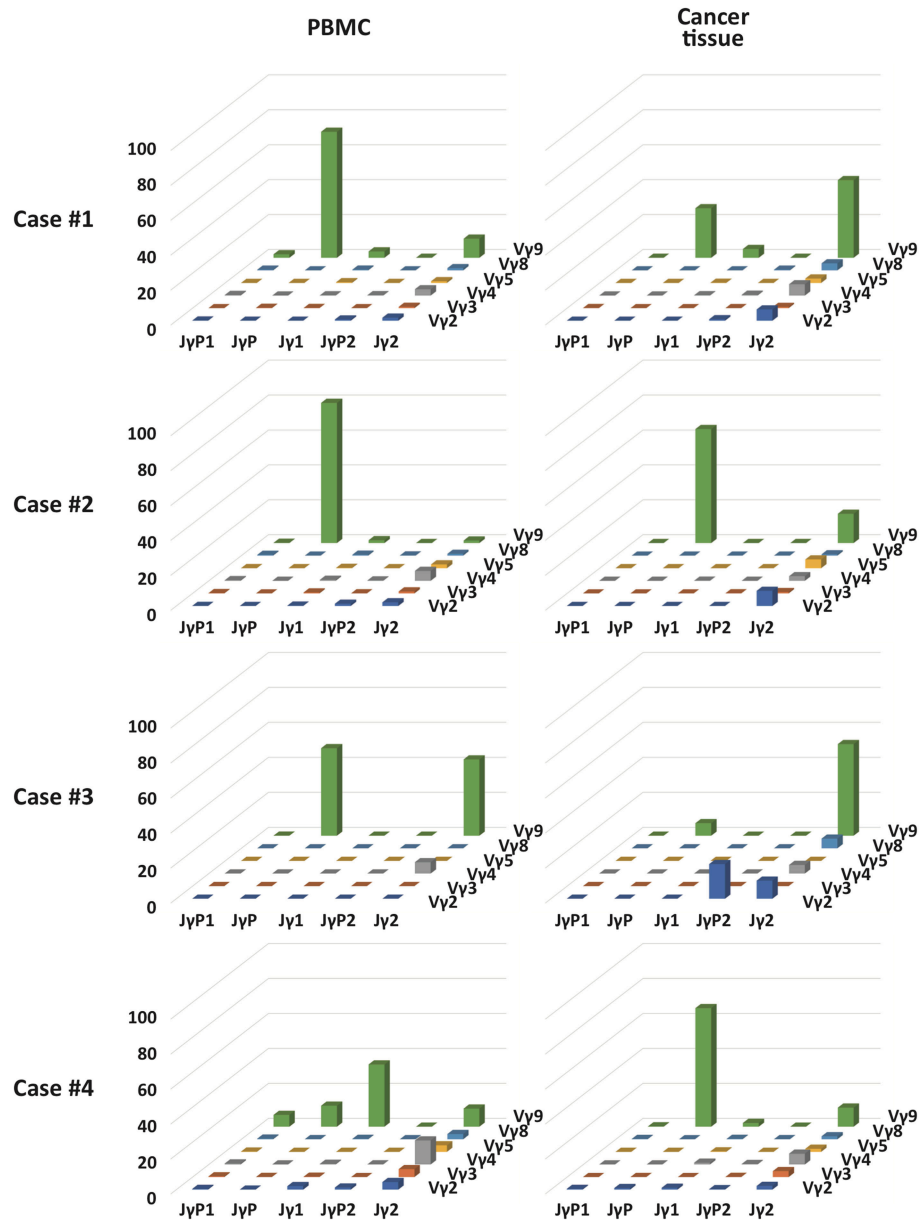


**FIGURE 4 |** The relative proportion of each combination of V $\gamma$  and J $\gamma$  segments in  $\gamma\delta$  T cells in blood and GBM tumor tissue samples of four patients. 3D graphs show the relative percentages of combinations of V $\gamma$ -J $\gamma$  usages in PBMCs or GBM tumor tissues from four patients.

this clonotype appeared to be recruited to the tumor tissues from the blood.

## DISCUSSION

In this study, we investigated the  $\gamma\delta$  TCR repertoires in tumor tissues and matched blood from four patients with IDH1 wild-type GBM. Except in one case, unique tumor-infiltrating GBM-specific  $\gamma\delta$  T cells used V $\gamma$ 9J $\gamma$ 2 sequences whereas blood  $\gamma\delta$  T cells were dominated by  $\gamma\delta$  T cells with V $\gamma$ 9J $\gamma$ P sequences. Based on the TCR $\gamma$  gene structure,

V $\gamma$ 9V $\delta$ 2 T cells with V $\gamma$ 9J $\gamma$ 2 sequences should use the C $\gamma$ 2 segment, whereas canonical  $\gamma\delta$  T cells with V $\gamma$ 9J $\gamma$ P sequences found predominantly in the blood are presumed to be C $\gamma$ 1 users as the J $\gamma$ P segment is much closer to the C $\gamma$ 1 segment than to the C $\gamma$ 2 segment. Because  $\gamma\delta$  T cells developed sequentially from C $\gamma$ 1-dependent proximal rearrangement to C $\gamma$ 2-dependent distal rearrangement (32, 60), these two types of V $\gamma$ 9V $\delta$ 2 T cells appear to have developed in different developmental stages.

Upon antigen stimulation,  $\gamma\delta$  T cells differentiate into two major types of memory T cells: central memory cells, which

**TABLE 3 |** TOP 10 CDR3 sequence by the usage proportion of V $\gamma$ 9J $\gamma$ 2 or V $\gamma$ 9J $\gamma$ P in patient blood and tissue sample.

CASE #1		PBMCs		Tissue		
V $\gamma$ 9 J $\gamma$ 2	CDR3 amino acid sequence	% of V $\gamma$ 9J $\gamma$ 2 sequences	% of total sequences	CDR3 amino acid sequence	% of V $\gamma$ 9J $\gamma$ 2 sequences	% of total sequences
1	ALWARLYYKKL	17.86	1.96	ALWEVRYYYKKL	27.19	12.09
2	ALWEVQPPYKKL	5.47	0.60	ALWARLYYKKL	12.03	5.35
3	ALWEVSLYKKL	5.32	0.58	ALWECHYYKKL	6.81	3.03
4	ALWEVAPLYKKL	4.82	0.53	ALWEGNYYKKL	3.92	1.74
5	ALWESPYKKL	4.35	0.48	ALWEAPKNTL	3.61	1.60
6	ALARKKL	4.31	0.47	ALWEGVNYYKKL	3.51	1.56
7	ALWEVLRYYKKL	4.29	0.47	ALWEVQF	3.43	1.52
8	ALWDKKL	4.25	0.47	ALWEVLLEKL	3.24	1.44
9	ALWNKKL	4.20	0.46	ALWEVPYYKKL	2.86	1.27
10	ALWEVRAWYYKKL	4.17	0.46	ALWYYKKL	2.85	1.27
V $\gamma$ 9 J $\gamma$ P	CDR3 amino acid sequence	% of V $\gamma$ 9J $\gamma$ P sequences	% of total sequences	CDR3 amino acid sequence	% of V $\gamma$ 9J $\gamma$ P sequences	% of total sequences
1	ALWEVQELGKKIKV	17.76	12.83	ALWEVQELGKKIKV	5.14	5.14
2	ALWEVRELGKKIKV	5.31	3.83	ALWEVRELGKKIKV	3.83	3.83
3	ALWEVQRELGKKIKV	3.04	2.20	ALWEDQELGKKIKV	2.16	2.16
4	ALWEPLGELGKKIKV	2.75	1.98	ALWDKQELGKKIKV	1.57	1.57
5	ALWEELGKKIKV	2.71	1.96	ALWWELGKKIKV	1.43	1.43
6	ALWEAQELGKKIKV	2.68	1.93	ALWEVMELGKKIKV	1.36	1.36
7	ALWEVQGLGKKIKV	2.49	1.80	ALWEPPELGKKIKV	1.35	1.35
8	ALWEEKELGKKIKV	2.30	1.66	ALWAVELGKKIKV	1.25	1.25
9	ALWDKQELGKKIKV	2.26	1.63	ALLGKKIKV	1.18	1.18
10	ALWEVRRELGKKIKV	2.21	1.59	ALWEVNQELGKKIKV	1.09	1.09
CASE #2		PBMCs		Tissue		
V $\gamma$ 9 J $\gamma$ 2	CDR3 amino acid sequence	% of V $\gamma$ 9J $\gamma$ 2 sequences	% of total sequences	CDR3 amino acid sequence	% of V $\gamma$ 9J $\gamma$ 2 sequences	% of total sequences
1	ALWEAPVEKL	26.04	0.37	ALWEGLKKL	17.58	2.95
2	ALSMQSFYKKL	16.47	0.23	AFENYKKL	17.07	2.87
3	ALWEGPKKL	16.19	0.23	ALEDKL	15.50	2.60
4	ALWEEDPDYKKL	13.80	0.19	ALWEVYV	15.35	2.58
5	ALWEVPAGYKKL	12.40	0.17	ALWEVLYKKL	13.62	2.29
6	ALWEVRDYKKL	6.69	0.09	ALSNYKKL	13.32	2.24
7	ALWRIYYKKL	4.15	0.06	ALWEFLYWGKL	5.38	0.90
8	ALGGGKL	3.60	0.05	ALEDKF	0.66	0.11
9	ALWEASVEKL	0.15	0.00	ALGDKL	0.47	0.08
10	ALGGGKF	0.13	0.00	ALEDRL	0.15	0.03
V $\gamma$ 9 J $\gamma$ P	CDR3 amino acid sequence	% of V $\gamma$ 9J $\gamma$ P sequences	% of total sequences	CDR3 amino acid sequence	% of V $\gamma$ 9J $\gamma$ P sequences	% of total sequences
1	ALWEPPQELGKKIKV	22.95	18.42	ALWEPPQELGKKIKV	31.41	20.52
2	ALWEYRQELGKKIKV	8.59	6.89	ALWERELGKKIKV	9.49	6.20
3	ALWEVQELGKKIKV	8.34	6.70	ALWEVEELGKKIKV	8.13	5.31
4	ALWEAQELGKKIKV	7.64	6.13	ALWEVQELGKKIKV	7.65	4.99
5	ALWEVEELGKKIKV	6.15	4.94	ALWEPQELGKKIKV	6.75	4.41
6	ALWEPQELGKKIKV	5.70	4.58	ALWEDNSPKLGKKIKV	4.50	2.94
7	ALWELLEQELGKKIKV	4.91	3.94	ALWERQELGKKIKV	4.25	2.78

(Continued)

TABLE 3 | Continued

<b>V<math>\gamma</math>9 JyP</b>	<b>CDR3 amino acid sequence</b>	<b>% of V<math>\gamma</math>9JyP sequences</b>	<b>% of total sequences</b>	<b>CDR3 amino acid sequence</b>	<b>% of V<math>\gamma</math>9JyP sequences</b>	<b>% of total sequences</b>
8	ALWEVPRELGKKIKV	3.68	2.95	ALWAQELGKKIKV	4.05	2.65
9	ALWEGEQELGKKIKV	2.88	2.32	ALWELLEQELGKKIKV	4.03	2.64
10	ALWEVQEELGKKIKV	2.50	2.01	ALWEGRELGKKIKV	4.03	2.63
<b>CASE #3</b>		<b>PBMCs</b>		<b>Tissue</b>		
<b>V<math>\gamma</math>9 Jy2</b>	<b>CDR3 amino acid sequence</b>	<b>% of V<math>\gamma</math>9Jy2 sequences</b>	<b>% of total sequences</b>	<b>CDR3 amino acid sequence</b>	<b>% of V<math>\gamma</math>9Jy2 sequences</b>	<b>% of total sequences</b>
1	ALWESSNYYKKL	98.22	42.79	ALWEVQYKKL	55.75	29.18
2	ALWEPNYYKKL	0.44	0.19	ALWEHYKKL	31.20	16.33
3	ALWGSSNYYKKL	0.33	0.14	ALWEVREKL	12.08	6.32
4	ALWESSYYKKL	0.26	0.11	ALWGHYYKKL	0.21	0.11
5	ALWESPYYKKL	0.21	0.09	ALWEVREEL	0.18	0.10
6	ALCESSNYYKKL	0.21	0.09	ALWEVQHKKL	0.10	0.05
7	ALWESSDYKKL	0.15	0.07	ALWEYYKKL	0.08	0.04
8	ALWKSSNYYKKL	0.07	0.03	ALWEHHYKKL	0.07	0.04
9	ALWVSSNYYKKL	0.04	0.02	ALWEVQCKKL	0.07	0.04
10	ALWESSYYKKL	0.01	0.01	ALWEMQYKKL	0.04	0.02
<b>V<math>\gamma</math>9 JyP</b>	<b>CDR3 amino acid sequence</b>	<b>% of V<math>\gamma</math>9JyP sequences</b>	<b>% of total sequences</b>	<b>CDR3 amino acid sequence</b>	<b>% of V<math>\gamma</math>9JyP sequences</b>	<b>% of total sequences</b>
1	ALWEKQELGKKIKV	98.65	49.31	ALWAQELGKKIKV	96.51	6.89
2	ALWEEQELGKKIKV	0.34	0.17	ALGAQELGKKIKV	2.17	0.15
3	ALWKGQELGKKIKV	0.26	0.13	ALWAQGLGKKIKV	0.37	0.03
4	ALWERQELGKKIKV	0.26	0.13	ALWARELGKKIKV	0.27	0.02
5	ALWEKRELGKKIKV	0.23	0.12	ALFAQELGKKIKV	0.24	0.02
6	ALWEKQKLGKKIKV	0.05	0.03	ALWTQELGKKIKV	0.21	0.02
7	ALWKKQELGKKIKV	0.05	0.03	ALWAQVLGKKIKV	0.08	0.01
8	ALWVKQELGKKIKV	0.03	0.01	ALWPQELGKKIKV	0.06	0.00
9	ALWEKHELGKKIKV	0.02	0.01	ALWAQKLGKKIKV	0.05	0.00
10	ALCEKQELGKKIKV	0.02	0.01	ALWAQEVGKKIKV	0.04	0.00
<b>CASE #4</b>		<b>PBMCs</b>		<b>Tissue</b>		
<b>V<math>\gamma</math>9 Jy2</b>	<b>CDR3 amino acid sequence</b>	<b>% of V<math>\gamma</math>9Jy2 sequences</b>	<b>% of total sequences</b>	<b>CDR3 amino acid sequence</b>	<b>% of V<math>\gamma</math>9Jy2 sequences</b>	<b>% of total sequences</b>
1	ALWEVQLPNYYKKL	24.75	2.56	ASKTKKLL	14.06	1.53
2	ALWEKSKNYYKKL	17.20	1.78	ALWEGENYYKKL	9.58	1.04
3	ALWEVLYKKL	7.02	0.73	ALWEVWRKL	6.03	0.66
4	ALWEVMDYKKL	4.23	0.44	ALWGRNYYKKL	5.07	0.55
5	ALWESEVISNYYKKL	4.10	0.42	ALWEVRFYKKL	4.73	0.52
6	ALWEVMNKKL	3.92	0.40	ALWEVLLNYYKKL	4.63	0.50
7	ACYKKL	3.71	0.38	ALWEVPDYKKL	4.11	0.45
8	ALWEVPEKL	3.34	0.35	ALWEVDYKKL	4.09	0.44
9	ALWEAGNYYKKL	3.12	0.32	ALWETVKKL	4.07	0.44
10	ALWDVRL	2.81	0.29	ALWEDLGKL	3.79	0.41
<b>V<math>\gamma</math>9 JyP</b>	<b>CDR3 amino acid sequence</b>	<b>% of V<math>\gamma</math>9JyP sequences</b>	<b>% of total sequences</b>	<b>CDR3 amino acid sequence</b>	<b>% of V<math>\gamma</math>9JyP sequences</b>	<b>% of total sequences</b>
1	ALWEALRLGKKIKV	31.84	3.81	ALWESQELGKKIKV	44.74	30.35
2	ALWEVQELGKKIKV	13.09	1.57	ALWDSYGLGKKIKV	15.55	10.55
3	ALWEQELGKKIKV	13.04	1.56	ALWEVQELGKKIKV	14.28	9.69

(Continued)

TABLE 3 | Continued

V $\gamma$ 9 J $\gamma$ P	CDR3 amino acid sequence	% of V $\gamma$ 9J $\gamma$ P sequences	% of total sequences	CDR3 amino acid sequence	% of V $\gamma$ 9J $\gamma$ P sequences	% of total sequences
4	ALWGQELGKKIKV	5.92	0.71	ALWGQELGKKIKV	9.58	6.50
5	ALWGSELGKKIKV	5.12	0.61	ALWEVQELGKKIKV	8.13	5.51
6	ALWESQELGKKIKV	4.92	0.59	ALWEQELGKKIKV	3.94	2.67
7	ALQELGKKIKV	4.81	0.58	ALWEIFQELGKKIKV	1.16	0.79
8	ALWEVQELGKKIKV	4.45	0.53	ALWETQELGKKIKV	1.10	0.75
9	ALWEIFQELGKKIKV	4.28	0.51	ALWEVFEQELGKKIKV	0.58	0.40
10	ALWDSYGLGKKIKV	2.28	0.27	ALWEVQELGKKIKV	0.36	0.24

patrol the blood and secondary lymphoid organs, and effector memory cells, which migrate to peripheral tissues (52). The circulating V $\gamma$ 9V $\delta$ 2 T cells preferentially express inflammatory homing chemokine receptors including CC chemokine receptor (CCR)1, CCR5, CCR8, CXCR3, and C-X-C chemokine receptor type 4 (CXCR4), which are involved in cell migration from the bloodstream to the tumor site, where they display broad and potent antitumoral activity (61–64). Then, activated V $\gamma$ 9V $\delta$ 2 T cells are able to secrete chemokines, such as chemokine ligands (CCL)3, CCL4, chemokine (C-X-C motif) ligand (CXCL)10, and CXCL13, to recruit dendritic cells/macrophages, NK cells,  $\alpha\beta$  T cells and B cells to the tumor site (53, 65). V $\gamma$ 9V $\delta$ 2 T cells can directly kill tumor cells through the secretion of cytolytic molecules or antibody-dependent cell-mediated cytotoxicity or indirectly prime and modulate immunological functions of other innate and adaptive immune cells leading to the establishment of profound antitumor immunity (53, 66, 67). For example, upon pAg stimulation, V $\gamma$ 9V $\delta$ 2 T cells preferentially differentiate into Th1-like cells with profound interferon- $\gamma$  and tumor necrosis factor- $\alpha$  responses (49, 54). However, upon stimulation with IPP, V $\gamma$ 9V $\delta$ 2 T cells can also be polarized into Th2-like cells, which are characterized by increased secretion of interleukin (IL)-4 upon stimulation with IL-4 and anti-IL-12 antibodies (54) and Treg-like  $\gamma\delta$ -T cells with regulatory/immunosuppressive functions in the presence of IL-15 and transforming growth factor- $\beta$  (55), displaying the functions for promoting tumor development through direct or indirect strategies. To date, it is not known whether these protumor V $\gamma$ 9V $\delta$ 2 T cells have the same clonotypes as antitumor V $\gamma$ 9V $\delta$ 2 T cells. Classical immunotherapeutic approaches to GBM have shown mixed results, and therapies focused on innate lymphocyte activity against GBM have not been rigorously evaluated. The adoption of V $\gamma$ 9V $\delta$ 2 T cells with both canonical and non-canonical V $\gamma$ 9V $\delta$ 2 T cells needs to be evaluated in GBM immunotherapy.

The binding between canonical V $\gamma$ 9V $\delta$ 2 TCR and pAgs presented by BTN3A1 leads to activation of V $\gamma$ 9V $\delta$ 2 T cells (18, 21). Microbe-derived hydroxymethyl-but-2-enyl-pyrophosphate (HMBPP) is  $\sim$ 10,000-fold more potent than cancer cell-derived IPP in the activation of V $\gamma$ 9V $\delta$ 2 T cells (18), but it is not understood how HMBPP triggers stronger signaling in V $\gamma$ 9V $\delta$ 2 T cells than IPP. CDR3 $\gamma$  appeared to

be essential for recognition of pyrophosphate-containing metabolites by BTN3A1. In particular, Lys109 in the CDR3 $\gamma$  from the J $\gamma$ P segment was shown to be critical for the binding (68). The CDR3 $\gamma$  sequences from V $\gamma$ 9J $\gamma$ 2-V $\delta$ 2 T cells showed a shorter length than the CDR3 $\gamma$  sequences from canonical V $\gamma$ 9V $\delta$ 2 T cells with V $\gamma$ 9J $\gamma$ P sequences, and some clonotypes from V $\gamma$ 9V $\delta$ 2 T cells with V $\gamma$ 9J $\gamma$ 2 sequences lacked the critical Lys residue (**Supplementary Figure 3**). Therefore, further studies are needed to determine whether intratumoral V $\gamma$ 9J $\gamma$ 2-V $\delta$ 2 T cells recognize the same antigens that bind to the canonical V $\gamma$ 9V $\delta$ 2 T cells with V $\gamma$ 9J $\gamma$ P sequences with similar affinities.

Collectively, our data showed that the TCR repertoires of intratumoral  $\gamma\delta$  T cells were clearly distinct from those of blood  $\gamma\delta$  T cells when comparing TCR repertoires from four patients with GBM. We also identified several GBM-specific V $\gamma$ 9J $\gamma$ 2-V $\delta$ 2 T cells that were not found in the blood. In-depth investigation of their antigenic specificities and anti- or protumor differentiation potentials through interaction with tumor cells and other stromal cells within GBM-specific TME should be performed to improve our understanding of the roles of  $\gamma\delta$  T cells in the establishment of the TME and to apply them for the future immunotherapies against GBMs refractory to conventional immunotherapies.

## AUTHOR CONTRIBUTIONS

D-SK, HL, and TK contributed to the conception and design of the study. ML, CP, JW, D-SK, HL, and TK developed the methodology of the study. ML, CP, JW, JK, IK, D-HN, W-YP, and Y-SK acquired the data, analyzed and interpreted the data. ML, CP, JW, D-SK, HL, and TK wrote the first draft of the manuscript. HL and TK wrote the final form of the manuscript. D-SK, HL, and TK supervised the overall study.

## ACKNOWLEDGMENTS

This research was partially funded by grants from the Korea Health Technology R&D Project through the Korea Health Industry Development Institute (KHIDI), funded by the Ministry of Health & Welfare, Republic of Korea (HI14C3418), Samsung Medical Center grant, Basic Science Research

Program through the National Research Foundation of Korea (NRF), funded by the Ministry of Education, (NRF-2017R1A2B4011780) and Ministry of Science, ICT and Future Planning (NRF-2016R1A5A2945889, NRF-2015M3A9B5053642, and NRF-2015M3A9B5052903).

## SUPPLEMENTARY MATERIAL

The Supplementary Material for this article can be found online at: <https://www.frontiersin.org/articles/10.3389/fimmu.2019.00555/full#supplementary-material>

## REFERENCES

- Parney IF, Waldron JS, Parsa AT. Flow cytometry and *in vitro* analysis of human glioma-associated macrophages. Laboratory investigation. *J Neurosurg.* (2009) 110:572–82. doi: 10.3171/2008.7.JNS08475
- Giering A, Kaminska B. Myeloid-derived suppressor cells in gliomas. *Contemp Oncol.* (2016) 20:345–51. doi: 10.5114/wo.2016.64592
- Fecci PE, Mitchell DA, Whitesides JF, Xie W, Friedman AH, Archer GE, et al. Increased regulatory T-cell fraction amidst a diminished CD4 compartment explains cellular immune defects in patients with malignant glioma. *Cancer Res.* (2006) 66:3294–302. doi: 10.1158/0008-5472.CAN-05-3773
- Lohr J, Ratliff T, Huppertz A, Ge Y, Dictus C, Ahmadi R, et al. Effector T-cell infiltration positively impacts survival of glioblastoma patients and is impaired by tumor-derived TGF- $\beta$ . *Clin Cancer Res.* (2011) 17:4296–308. doi: 10.1158/1078-0432.CCR-10-2557
- Rooney MS, Shukla SA, Wu CJ, Getz G, Hacohen N. Molecular and genetic properties of tumors associated with local immune cytolytic activity. *Cell.* (2015) 160:48–61. doi: 10.1016/j.cell.2014.12.033
- Wang Q, Hu B, Hu X, Kim H, Squatrito M, Scarpace L, et al. Tumor evolution of glioma-intrinsic gene expression subtypes associates with immunological changes in the microenvironment. *Cancer Cell.* (2017) 32:42–56 e6. doi: 10.1016/j.ccell.2017.06.003
- Wang J, Cazzato E, Ladewig E, Frattini V, Rosenbloom DI, Zairis S, et al. Clonal evolution of glioblastoma under therapy. *Nat Genet.* (2016) 48:768–76. doi: 10.1038/ng.3590
- Gabrusiewicz K, Ellert-Miklaszewska A, Lipko M, Sielska M, Frankowska M, Kaminska B. Characteristics of the alternative phenotype of microglia/macrophages and its modulation in experimental gliomas. *PLoS ONE.* (2011) 6:e23902. doi: 10.1371/journal.pone.0023902
- Giering A, Pszczolkowska D, Bocian K, Dabrowski M, Rajan WD, Kloss M, et al. Immune microenvironment of experimental rat C6 gliomas resembles human glioblastomas. *Sci Rep.* (2017) 7:17556. doi: 10.1038/s41598-017-17752-w
- Chanmee T, Ontong P, Konno K, Itano N. Tumor-associated macrophages as major players in the tumor microenvironment. *Cancers.* (2014) 6:1670–90. doi: 10.3390/cancers6031670
- Piao Y, Liang J, Holmes L, Zurita AJ, Henry V, Heymach JV, et al. Glioblastoma resistance to anti-VEGF therapy is associated with myeloid cell infiltration, stem cell accumulation, and a mesenchymal phenotype. *Neuro Oncol.* (2012) 14:1379–92. doi: 10.1093/neuonc/nos158
- Lim M, Xia Y, Bettgeoda C, Weller M. Current state of immunotherapy for glioblastoma. *Nat Rev Clin Oncol.* (2018) 15:422–42. doi: 10.1038/s41571-018-0003-5
- Fournie JJ, Sicard H, Poupot M, Bezombes C, Blanc A, Romagne F, et al. What lessons can be learned from gammadelta T cell-based cancer immunotherapy trials? *Cell Mol Immunol.* (2013) 10:35–41. doi: 10.1038/cmi.2012.39
- Bryant NL, Suarez-Cuervo C, Gillespie GY, Markert JM, Nabors LB, Meleth S, et al. Characterization and immunotherapeutic potential of gammadelta T-cells in patients with glioblastoma. *Neuro Oncol.* (2009) 11:357–67. doi: 10.1215/15228517-2008-111
- Correia DV, Lopes A, Silva-Santos B. Tumor cell recognition by gammadelta T lymphocytes: T-cell receptor vs. NK-cell receptors. *Oncoimmunology.* (2013) 2:e22892. doi: 10.4161/onci.22892
- Bonneville M, O'Brien RL, Born WK. Gammadelta T cell effector functions: a blend of innate programming and acquired plasticity. *Nat Rev Immunol.* (2010) 10:467–78. doi: 10.1038/nri2781
- Vantourout P, Hayday A. Six-of-the-best: unique contributions of gammadelta T cells to immunology. *Nat Rev Immunol.* (2013) 13:88–100. doi: 10.1038/nri3384
- Gu S, Nawrocka W, Adams EJ. Sensing of pyrophosphate metabolites by Vgamma9Vdelta2 T Cells. *Front Immunol.* (2014) 5:688. doi: 10.3389/fimmu.2014.00688
- Chitadze G, Lettau M, Luecke S, Wang T, Janssen O, Furst D, et al. NKG2D- and T-cell receptor-dependent lysis of malignant glioma cell lines by human gammadelta T cells: Modulation by temozolomide and A disintegrin and metalloproteases 10 and 17 inhibitors. *Oncoimmunology.* (2016) 5:e1093276. doi: 10.1080/2162402X.2015.1093276
- Lefranc MP. The human T-cell rearranging gamma (TRG) genes and the gamma T-cell receptor. *Biochimie.* (1988) 70:901–8.
- Vavassori S, Kumar A, Wan GS, Ramanjaneyulu GS, Cavallari M, El Daker S, et al. Butyrophilin 3A1 binds phosphorylated antigens and stimulates human gammadelta T cells. *Nat Immunol.* (2013) 14:908–16. doi: 10.1038/ni.2665
- Gober HJ, Kistowska M, Angman L, Jeno P, Mori L, De Libero G. Human T cell receptor gammadelta cells recognize endogenous mevalonate metabolites in tumor cells. *J Exp Med.* (2003) 197:163–8. doi: 10.1084/jem.20021500
- Thompson K, Dunford JE, Ebetino FH, Rogers MJ. Identification of a bisphosphonate that inhibits isopentenyl diphosphate isomerase and farnesyl diphosphate synthase. *Biochem Biophys Res Commun.* (2002) 290:869–73. doi: 10.1006/bbrc.2001.6289
- Kong Y, Cao W, Xi X, Ma C, Cui L, He W. The NKG2D ligand ULBP4 binds to TCRgamma9/delta2 and induces cytotoxicity to tumor cells through both TCRgammadelta and NKG2D. *Blood.* (2009) 114:310–7. doi: 10.1182/blood-2008-12-196287
- Dai Y, Chen H, Mo C, Cui L, He W. Ectopically expressed human tumor biomarker MutS homologue 2 is a novel endogenous ligand that is recognized by human gammadelta T cells to induce innate anti-tumor/virus immunity. *J Biol Chem.* (2012) 287:16812–9. doi: 10.1074/jbc.M111.327650
- Vantourout P, Mookerjee-Basu J, Rolland C, Pont F, Martin H, Davrinche C, et al. Specific requirements for Vgamma9Vdelta2 T cell stimulation by a natural adenylated phosphoantigen. *J Immunol.* (2009) 183:3848–57. doi: 10.4049/jimmunol.0901085
- Zitvogel L, Apetoh L, Ghiringhelli F, Kroemer G. Immunological aspects of cancer chemotherapy. *Nat Rev Immunol.* (2008) 8:59–73. doi: 10.1038/nri2216
- Robins H. Immunosequencing: applications of immune repertoire deep sequencing. *Curr Opin Immunol.* (2013) 25:646–52. doi: 10.1016/j.coi.2013.09.017
- Emerson RO, Sherwood AM, Rieder MJ, Guenther J, Williamson DW, Carlson CS, et al. High-throughput sequencing of T-cell receptors reveals a homogeneous repertoire of tumour-infiltrating lymphocytes in ovarian cancer. *J Pathol.* (2013) 231:433–40. doi: 10.1002/path.4260
- Chien YH, Bonneville M. Gamma delta T cell receptors. *Cell Mol Life.* (2006) 63:2089–94. doi: 10.1007/s00018-006-6020-z
- Borst J, Wicherink A, Van Dongen JJ, De Vries E, Comans-Bitter WM, Wassenaar F, et al. Non-random expression of T cell receptor gamma and delta variable gene segments in functional T lymphocyte clones from human peripheral blood. *Eur J Immunol.* (1989) 19:1559–68. doi: 10.1002/eji.1830190907
- Tribel F, Lefranc MP, Hercend T. Further evidence for a sequentially ordered activation of T cell rearranging gamma genes during T lymphocyte differentiation. *Eur J Immunol.* (1988) 18:789–94. doi: 10.1002/eji.1830180520
- Chen H, He X, Wang Z, Wu D, Zhang H, Xu C, et al. Identification of human T cell receptor gammadelta-recognized epitopes/proteins via CDR3delta peptide-based immunobiochemical strategy. *J Biol Chem.* (2008) 283:12528–37. doi: 10.1074/jbc.M708067200
- Xi X, Guo Y, Chen H, Xu C, Zhang H, Hu H, et al. Antigen specificity of gammadelta T cells depends primarily on the flanking sequences of CDR3delta. *J Biol Chem.* (2009) 284:27449–55. doi: 10.1074/jbc.M109.011684

35. Dobin A, Davis CA, Schlesinger F, Drenkow J, Zaleski C, Jha S, et al. STAR: ultrafast universal RNA-seq aligner. *Bioinformatics*. (2013) 29:15–21. doi: 10.1093/bioinformatics/bts635
36. Li B, Dewey CN. RSEM: accurate transcript quantification from RNA-Seq data with or without a reference genome. *BMC Bioinformatics*. (2011) 12:323. doi: 10.1186/1471-2105-12-323
37. Newman AM, Liu CL, Green MR, Gentles AJ, Feng W, Xu Y, et al. Robust enumeration of cell subsets from tissue expression profiles. *Nat Methods*. (2015) 12:453–7. doi: 10.1038/nmeth.3337
38. Azizi E, Carr AJ, Plitas G, Cornish AE, Konopacki C, Prabhakaran S, et al. Single-cell map of diverse immune phenotypes in the breast tumor microenvironment. *Cell*. (2018) 174:1293–308 e36. doi: 10.1016/j.cell.2018.05.060
39. Chung W, Eum HH, Lee HO, Lee HB, Kim KT, et al. Single-cell RNA-seq enables comprehensive tumour and immune cell profiling in primary breast cancer. *Nat Commun*. (2017) 8:15081. doi: 10.1038/ncomms15081
40. De Simone M, Arrigoni A, Rossetti G, Gruarin P, Ranzani V, Politano C, et al. Transcriptional landscape of human tissue lymphocytes unveils uniqueness of tumor-infiltrating T regulatory cells. *Immunity*. (2016) 45:1135–47. doi: 10.1016/j.immuni.2016.10.021
41. Finotello F, Trajanoski Z. Quantifying tumor-infiltrating immune cells from transcriptomics data. *Cancer Immunol Immunother*. (2018) 67:1031–40. doi: 10.1007/s00262-018-2150-z
42. Hanzelmann S, Castelo R, Guinney J. GSEA: gene set variation analysis for microarray and RNA-seq data. *BMC Bioinformatics*. (2013) 14:7. doi: 10.1186/1471-2105-14-7
43. GR Warnes BB, L Bonebakker, R Gentleman, WHA Liaw, T Lumley. *gplots: Various R Programming Tools for Plotting Data*. R package version 2.12. 1. 2013. *Google Scholar* (2014).
44. Giudicelli V, Duroux P, Ginestoux C, Folch G, Jabado-Michaloud J, Chaume D, et al. IMGT/LIGM-DB, the IMGT comprehensive database of immunoglobulin and T cell receptor nucleotide sequences. *Nucleic Acids Res*. (2006) 34:D781–4. doi: 10.1093/nar/gkj088
45. Li B, Li T, Pignon JC, Wang B, Wang J, Shukla SA, et al. Landscape of tumor-infiltrating T cell repertoire of human cancers. *Nat Genet*. (2016) 48:725–32. doi: 10.1038/ng.3581
46. Louis DN, Perry A, Reifenberger G, von Deimling A, Figarella-Branger D, Cavenee WK, et al. The 2016 World Health Organization classification of tumors of the central nervous system: a summary. *Acta Neuropathol*. (2016) 131:803–20. doi: 10.1007/s00401-016-1545-1
47. Stupp R, Mason WP, van den Bent MJ, Weller M, Fisher B, Taphoorn MJ, et al. Radiotherapy plus concomitant and adjuvant temozolomide for glioblastoma. *N Engl J Med*. (2005) 352:987–96. doi: 10.1056/NEJMoa043330
48. Tosolini M, Pont F, Pouput M, Vergez F, Nicolau-Travers ML, Vermijlen D, et al. Assessment of tumor-infiltrating TCRV $\gamma$ 9V $\delta$ 22 gammadelta lymphocyte abundance by deconvolution of human cancers microarrays. *Oncoimmunology*. (2017) 6:e1284723. doi: 10.1080/2162402X.2017.1284723
49. Dunne MR, Mangan BA, Madrigal-Estebas L, Doherty DG. Preferential Th1 cytokine profile of phosphoantigen-stimulated human V $\gamma$ 9V $\delta$ 22 T cells. *Mediators Inflamm*. (2010) 2010:704941. doi: 10.1155/2010/704941
50. Caccamo N, La Mendola C, Orlando V, Meraviglia S, Todaro M, Stassi G, et al. Differentiation, phenotype, and function of interleukin-17-producing human V $\gamma$ 9V $\delta$ 22 T cells. *Blood*. (2011) 118:129–38. doi: 10.1182/blood-2011-01-331298
51. Mao Y, Yin S, Zhang J, Hu Y, Huang B, Cui L, et al. A new effect of IL-4 on human gammadelta T cells: promoting regulatory V $\delta$ 1 T cells via IL-10 production and inhibiting function of V $\delta$ 22 T cells. *Cell Mol Immunol*. (2016) 13:217–28. doi: 10.1038/cmi.2015.07
52. Caccamo N, Todaro M, Sireci G, Meraviglia S, Stassi G, Dieli F. Mechanisms underlying lineage commitment and plasticity of human gammadelta T cells. *Cell Mol Immunol*. (2013) 10:30–4. doi: 10.1038/cmi.2012.42
53. Tyler CJ, Doherty DG, Moser B, Eberl M. Human V $\gamma$ 9V $\delta$ 22 T cells: Innate adaptors of the immune system. *Cell Immunol*. (2015) 296:10–21. doi: 10.1016/j.cellimm.2015.01.008
54. Wesch D, Glatzel A, Kabelitz D. Differentiation of resting human peripheral blood gamma delta T cells toward Th1- or Th2-phenotype. *Cell Immunol*. (2001) 212:110–7. doi: 10.1006/cimm.2001.1850
55. Casetti R, Agrati C, Wallace M, Sacchi A, Martini F, Martino A, et al. Cutting edge: TGF-beta1 and IL-15 Induce FOXP3+ gammadelta regulatory T cells in the presence of antigen stimulation. *J Immunol*. (2009) 183:3574–7. doi: 10.4049/jimmunol.0901334
56. Wu YL, Ding YP, Tanaka Y, Shen LW, Wei CH, Minato N, et al. gammadelta T cells and their potential for immunotherapy. *Int J Biol Sci*. (2014) 10:119–35. doi: 10.7150/ijbs.7823
57. De Rosa SC, Andrus JP, Perfetto SP, Mantovani JJ, Herzenberg LA, Herzenberg LA, et al. Ontogeny of gamma delta T cells in humans. *J Immunol*. (2004) 172:1637–45. doi: 10.4049/jimmunol.172.3.1637
58. Sherwood AM, Desmarais C, Livingston RJ, Andriesen J, Haussler M, Carlson CS, et al. Deep sequencing of the human TCRgamma and TCRbeta repertoires suggests that TCRbeta rearranges after alphabeta and gammadelta T cell commitment. *Sci Transl Med*. (2011) 3:90a61. doi: 10.1126/scitranslmed.3002536
59. Nazarov VI, Pogorelyy MV, Komech EA, Zvyagin IV, Bolotin DA, Shugay M, et al. tCR: an R package for T cell receptor repertoire advanced data analysis. *BMC Bioinformatics*. (2015) 16:175. doi: 10.1186/s12859-015-0613-1
60. Krangel MS, Yssel H, Brocklehurst C, Spits H. A distinct wave of human T cell receptor gamma/delta lymphocytes in the early fetal thymus: evidence for controlled gene rearrangement and cytokine production. *J Exp Med*. (1990) 172:847–59.
61. Bouet-Toussaint F, Cabillic F, Toutirais O, Le Gallo M, Thomas de la Pintiere C, Daniel P, et al. Vgamma9Vdelta2 T cell-mediated recognition of human solid tumors. Potential for immunotherapy of hepatocellular and colorectal carcinomas. *Cancer Immunol Immunother*. (2008) 57:531–9. doi: 10.1007/s00262-007-0391-3
62. Cipriani B, Borsellino G, Poccia F, Placido R, Tramonti D, Bach S, et al. Activation of C-C beta-chemokines in human peripheral blood gammadelta T cells by isopentenyl pyrophosphate and regulation by cytokines. *Blood*. (2000) 95:39–47.
63. Glatzel A, Wesch D, Schiemann F, Brandt E, Janssen O, Kabelitz D. Patterns of chemokine receptor expression on peripheral blood gamma delta T lymphocytes: strong expression of CCR5 is a selective feature of V delta 2/V gamma 9 gamma delta T cells. *J Immunol*. (2002) 168:4920–9. doi: 10.4049/jimmunol.168.10.4920
64. Hannani D, Ma Y, Yamazaki T, Dechanet-Merville J, Kroemer G, Zitvogel L. Harnessing gammadelta T cells in anticancer immunotherapy. *Trends Immunol*. (2012) 33:199–206. doi: 10.1016/j.it.2012.01.006
65. Conti L, Casetti R, Cardone M, Varano B, Martino A, Belardelli F, et al. Reciprocal activating interaction between dendritic cells and pamidronate-stimulated gammadelta T cells: role of CD86 and inflammatory cytokines. *J Immunol*. (2005) 174:252–60. doi: 10.4049/jimmunol.174.1.252
66. Ferreira LM. Gammadelta T cells: innately adaptive immune cells? *Int Rev Immunol*. (2013) 32:223–48. doi: 10.3109/08830185.2013.783831
67. Tokuyama H, Hagi T, Mattarollo SR, Morley J, Wang Q, So HF, et al. V gamma 9 V delta 2 T cell cytotoxicity against tumor cells is enhanced by monoclonal antibody drugs—rituximab and trastuzumab. *Int J Cancer*. (2008) 122:2526–34. doi: 10.1002/ijc.23365
68. Wang H, Fang Z, Morita CT. Vgamma2Vdelta2 T Cell Receptor recognition of prenyl pyrophosphates is dependent on all CDRs. *J Immunol*. (2010) 184:6209–22. doi: 10.4049/jimmunol.1000231

**Conflict of Interest Statement:** The authors declare that the research was conducted in the absence of any commercial or financial relationships that could be construed as a potential conflict of interest.

Copyright © 2019 Lee, Park, Woo, Kim, Kho, Nam, Park, Kim, Kong, Lee and Kim. This is an open-access article distributed under the terms of the Creative Commons Attribution License (CC BY). The use, distribution or reproduction in other forums is permitted, provided the original author(s) and the copyright owner(s) are credited and that the original publication in this journal is cited, in accordance with accepted academic practice. No use, distribution or reproduction is permitted which does not comply with these terms.